

NANO EXPRESS

Open Access



# Biogenic Synthesis, Characterization and Antibacterial Potential Evaluation of Copper Oxide Nanoparticles Against *Escherichia coli*

Mohsin Ali<sup>1</sup>, Muhammad Ijaz<sup>1\*</sup>, Muhammad Ikram<sup>2\*</sup> , Anwar Ul-Hamid<sup>3</sup>, Muhammad Avais<sup>1</sup> and Aftab Ahmad Anjum<sup>1</sup>

## Abstract

The development of resistance against antibiotics used to treat bacterial infections along with the prevalence of medication residues presents significant public health problems globally. Antibiotic-resistant germs result in infections that are difficult or impossible to treat. Decreasing antibiotic effectiveness calls for rapid development of alternative antimicrobials. In this respect, nanoparticles (NPs) of copper oxide (CuO) manifest a latent and flexible inorganic nanostructure with noteworthy antimicrobial impact. Green synthesis of CuO NPs was performed in the current study, which was then doped with varying amounts of ginger (*Zingiber officinale*, ZO) and garlic (*Allium sativum*, AS) extracts. In low and high doses, the synthesized compound was used to measure the antimicrobial effectiveness against pathogenic *Escherichia coli*. The present research successfully demonstrated a renewable, eco-friendly synthesis technique with natural materials that is equally applicable to other green metal oxide NPs.

**Keywords:** Bactericidal, Nanoparticles, Doping, *E. coli*, Mastitis, Biogenic synthesis, Ginger, Garlic

## Introduction

Indigenous herbal and spicy plants include valuable antioxidant and antibacterial properties that are employed in human and veterinary treatment [1]. Medicinal plants containing antimicrobial properties include garlic, ginger, neem, turmeric, tulsi, etc. and among these, garlic and ginger are famous for their medicinal use [2]. *Zingiber officinale* commonly known as ginger is an indigenous plant root belonging to Zingiberaceae family. It contains gingerol, shogaol, curcumin and paradol as important phytochemicals [3]. Antimicrobial activity against a wide range of microbes has been manifested by aqueous extracts of ginger, owing to its phenolic contents of therapeutic nature [4]. *Allium sativum* commonly known as

garlic contains phenolic compounds exhibiting a broad-spectrum antibacterial activity even against MDR bacteria [5]. *Allium sativum* has exhibited broad-spectrum antibacterial activity against a number of Gram-positive and various Gram-negative bacteria [6].

Exploiting the knowledge of nanotechnology at molecular and atomic levels serves as a basis to apply an integrative approach to develop novel compounds with unique features for use in broad-spectrum applications [7]. Medicinal, agricultural, food preservative and cosmetic applications of nanoparticles due to their unmatched inherent properties have led to an increased exploration by researchers [8, 9]. Various biological applications of copper oxide nanoparticles have been successfully demonstrated including potential antimicrobials, effective therapeutic compounds, drug delivery carriers, photocatalysts, gas sensing, photovoltaic stability, quantum confinement effect and biological probes [10–14]. Reactive oxygen species (ROS) generation is triggered by nanoparticles due to their

\*Correspondence: mijaz@uvas.edu.pk; dr.muhammadikram@gcu.edu.pk

<sup>1</sup> Department of Veterinary Medicine, University of Veterinary and Animal Sciences, Lahore, Punjab 54000, Pakistan

<sup>2</sup> Solar Cell Applications Research Lab, Department of Physics, Government College University Lahore, Lahore, Punjab 54000, Pakistan

Full list of author information is available at the end of the article

semiconductor nature, bringing oxidative and degenerative transformations at the cellular level resulting in destruction of bacterial cell walls and release of cellular contents [15]. Many methods have been practiced for the synthesis of nanoparticles, i.e., chemical, physical and biological synthesis [16]. Reduction of metallic compounds results in the production of nanoparticles using any biochemical or microorganism, plants or their extracts [17].

*Escherichia coli* (*E. coli*), a natural inhabitant of intestine and part of intestinal flora, has a distinctive position in microbiological world due to its potential virulent properties [18]. The existence of virulence depends on the number of genes in *E. coli* isolates and in some cases horizontal transfer of resistance genes has also been revealed [19, 20] which may create a health concern in human beings, animals [21] and challenge for food safety and security [22]. *E. coli* is causative agent of mastitis in dairy cows and buffaloes and was found responsible for a major decline in milk yield and consequent economic losses [23, 24], which developed resistance genes, i.e., extended-spectrum  $\beta$ -lactamases (ESBLs) or over-expressed cephalosporinases (AmpCs) [25]. Treatment failure associated with *E. coli* infections is considered as a latent threat leading to multidrug resistance both in human and veterinary medicines [26].

Nanoparticles with their characteristic antimicrobial features have the potential to kill around 600 cells in contrast to antibiotic's ability to treat only a few diseases of infectious origin [27]. The current study aims to explore, evaluate and compare the possible antimicrobial potential of green and chemically synthesized CuO nanoparticles and extracts of common herb roots of *Allium sativum* (AS) and *Zingiber officinale* (ZO), against pathogenic *E. coli* as alternatives to antibiotics to overcome the emerging resistance challenges.

## Methods

The current study was aimed at investigating the bactericidal action of phytochemically reduced CuO NPs against herb roots of *Allium sativum* (AS) and *Zingiber officinale* (ZO), an isolate of bovine mastitis.

## Materials

Chemically manufactured nanoparticles of CuO were procured from Sigma-Aldrich, whereas ZO and AS roots were acquired from local fruits and vegetable market of Lahore, Pakistan. Roots of ZO and AS were dried off under shade to attain even weight. Growth media for *E. coli* and analytical grade chemicals were utilized without modification.

## Aqueous Extraction of ZO and AS Roots

Dried roots of ZO and AS were ultrafine ground to fine powders that were then stored in airtight jars. Robust stirring of 30 min at 70 °C for mixing of fine powdered roots with distilled water-DIW was undertaken at 1:10 ratio. Filtration of the prepared solutions was performed using Whatman filter paper No. 1 after cooling the solutions and the storage of the filtrate was carried out at 4 °C for the next experiment [28] as exhibited in Fig. 1a.

## Green Synthesis of CuO

Cupric nitrate tetrahydrate (0.1 M) was blended with different concentrations, i.e., 3 mL, 6 mL and 12 mL of ZO and AS extracts under continuous stirring. NaOH (2 M) was used to maintain pH 12 of the stirred solution for 2 h at 90 °C for the formation of precipitates. Centrifugation of the precipitates was carried out at 10,000 rpm for 20 min, followed by DI water washing and overnight drying in a hot air oven at 90 °C [29] as portrayed in Fig. 1b.

## Characterization

UV–visible GENESYS-10S spectrophotometer was used to check the absorption spectra of CuO nanoparticles and aqueous extracts of ZO and AS between wavelengths range of 200 to 500 nm [30]. CuO NPs structural and phase analysis was performed using X-ray diffraction (XRD) BRUKER D2 Phaser with  $2\theta = (10^\circ - 80^\circ)$  equipped with Cu K $\alpha$  radiation of  $\lambda = 1.540 \text{ \AA}$  [31]. Fourier transform infrared spectroscopy (ATR-FTIR) was performed for the analysis of functional groups in CuO NPs and aqueous extracts of ZO and AS [31]. Scanning electron microscopy (JSM-6610LV SEM) coupled with EDS detector was undertaken for the observation of elemental and morphological constitution of CuO NPs. High-resolution TEM images and SAED patterns were taken using JEOL JEM-2100F microscope [32].

## *E. coli* Isolation and Identification

### Collection of Samples

Cows and buffaloes suffering from clinical mastitis were traced and identified from various livestock farms for the collection of milk samples.

### *E. coli* Isolation

MacConkey agar was used for streaking and culturing of milk in triplicate for isolation of purified colonies of *E. coli* [33]. Disk diffusions of distinctive colonies of *E. coli* were evaluated to check susceptibility against specific antibiotics observing the guidelines of the National

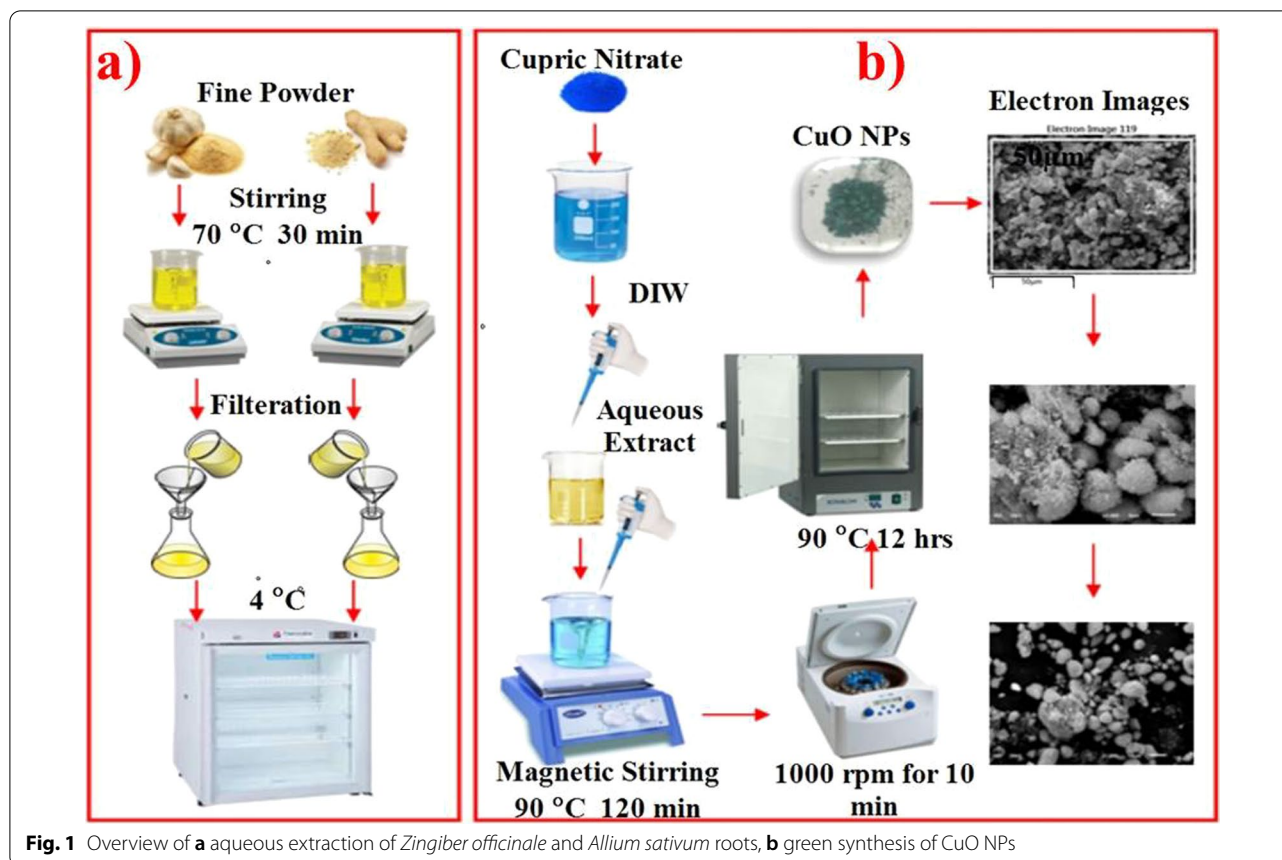


**Fig. 1** Overview of **a** aqueous extraction of *Zingiber officinale* and *Allium sativum* roots, **b** green synthesis of CuO NPs

Committee for Clinical Laboratory Standards (NCCLS) to isolate *E. coli*.

#### Identification of *E. coli*

Identification and confirmation of *E. coli* colonies were carried out based on Gram's staining; distinguishing morphological characters and biochemical tests, i.e., methyl red and catalase tests with perspective to the Bergey's Manual of Systematic Bacteriology. Culturing of isolates on eosin methylene blue (EMB) agar was performed for *E. coli* distinctness and ratification from related Gram-negative mastitogens.

#### Evaluation of CuO NPs In Vitro Antibacterial Potential Against *E. coli*

A number of experiments were performed to evaluate *in vitro* antibacterial potential of extract doped CuO NPs against pathogenic *E. coli*. *In vitro* trials were conducted using 10 representative pathogenic *E. coli* isolates for the evaluation of antibacterial potential of CuO NPs. Disk diffusion method assessment was used to assess *in vitro* antimicrobial potential. Petri dishes were swabbed with activated growth of *E. coli*  $1.5 \times 10^8$  CFU/mL (0.5 Mcfarland standard) on MacConkey agar [34]. A sterile cork

borer was used to prepare 6-mm-diameter wells in the petri dishes. Aqueous extracts of ZO and AS, along with green doped extracts and chemically synthesized copper oxide nanoparticles in different concentrations, were applied into wells. Antimicrobial potential of aqueous extracts of ZO and AS along with green doped extracts and chemically synthesized copper oxide nanoparticles was evaluated by aerobically incubating the petri dishes at 37 °C overnight by measuring the zones of inhibition (mm) using Vernier caliper. Statistical analysis of zones of inhibition (mm) was performed using one-way ANOVA and visualizing ( $p < 0.05$ ).

#### Results and Discussion

UV–Vis spectroscopy of doped CuO NPs and aqueous extracts of ZO and AS was accomplished to investigate the optical behavior as shown in Fig. 2a, b. For subsequent formation of CuO NPs, gradual color shift from wine to coal black was noticed while optimization of synthesized NPs by means of vaulted, acoustic extracts was undertaken. Aqueous extracts ZO and AS absorption peaks at 275 and 280 nm were observed. Results depicted  $\lambda_{\max}$  for ZO- and AS-doped CuO at 250 nm depicting ratio 6 mL:1 with characteristic redshifts and blueshifts,

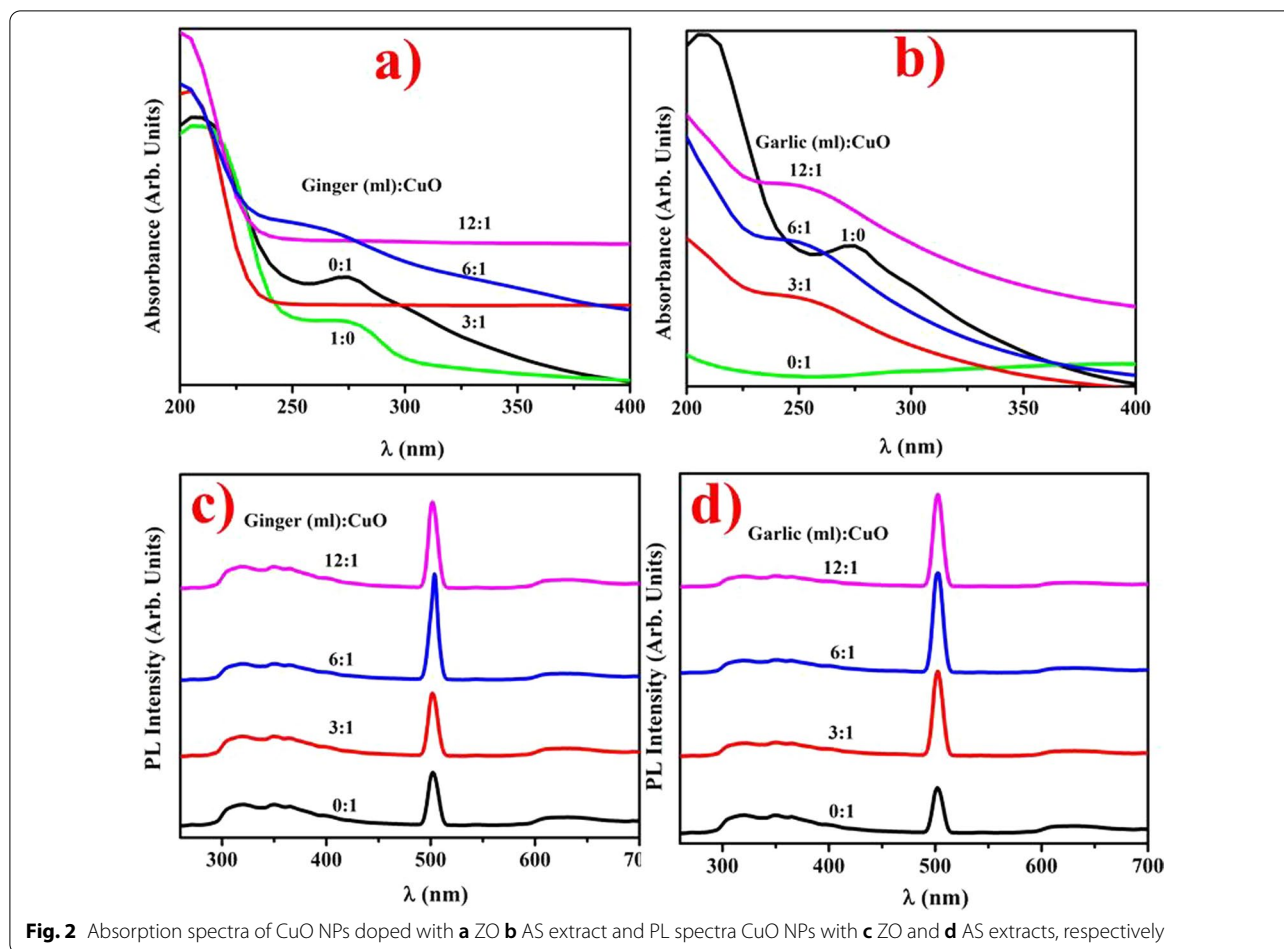


**Fig. 2** Absorption spectra of CuO NPs doped with **a** ZO **b** AS extract and PL spectra CuO NPs with **c** ZO and **d** AS extracts, respectively

respectively [35]. Wide peaks specified particle clusters and transition of electrons to conduction bands from valence phase with concentrated extracts in CuO as divulged by strong absorption bands [36]. In green synthesized CuO NPs, reduced absorption was seen by increasing or reducing extract volume in addition to the optimized value (6 mL:1).

Additionally, it was remarkable to observe that semi-conducting structures confirmed their physical features to the existing nanometric quantum-size effects. PL spectra of ZO- and AS-doped CuO NPs with exciting UV wavelength of 300 nm are presented in Fig. 2c, d. The three emission peaks at 418, 561 and 664 nm were represented on each pure and doped PL graph of CuO (UV region) [37]. A violet–blue light band found at 418 nm is a standard CuO emission peak at the near band edge [38, 39]. At 430 nm, the shoulder edge can be due to CuO vacancies, which is a p-type semiconductor. The yellowish green edge is responsible for the depth defects under low temperatures at 561 nm. The red emission peaks at 664 nm are responsible for different copper conditions or the presence of individual

ionized oxygen vacancies [40, 41]. The diverse existence of visible emissions in the violet–blue, yellow–green and red spectrum indicates that the studied CuO particles have a high volume–surface ratio and a multitude of surface-to-volume conditions and defects (vacancies or interstitials) that produce trap-to-emission ranges [40, 42].

XRD was performed to assess the crystalline structure, composition and scale of CuO NPs as presented in Fig. 3a, d doped with ZO and AS, respectively. The increase in crystallinity was demonstrated by peaks detected at  $2\theta = 38.7^\circ, 48.6^\circ, 53.5^\circ, 58.3^\circ, 61.7^\circ$  and  $66.2^\circ$  with corresponding crystal planes (111), (−202), (020), (202), (−113) and (022), respectively. The detected peaks assured the presence of CuO monoclinic phase as synchronized with JCPDS card no: 00–002–1040 [43]. The characteristic crystallite size measured using  $D = 0.9\lambda/\beta\cos\theta$  was found to be 24.7 and 47.6 nm for ZO- and AS-doped CuO, respectively, and pristine sample crystallite size was 27.4 nm. Several natural products have been identified as capping and reducing agents for average crystallite size in AS and ZO extracts [44].



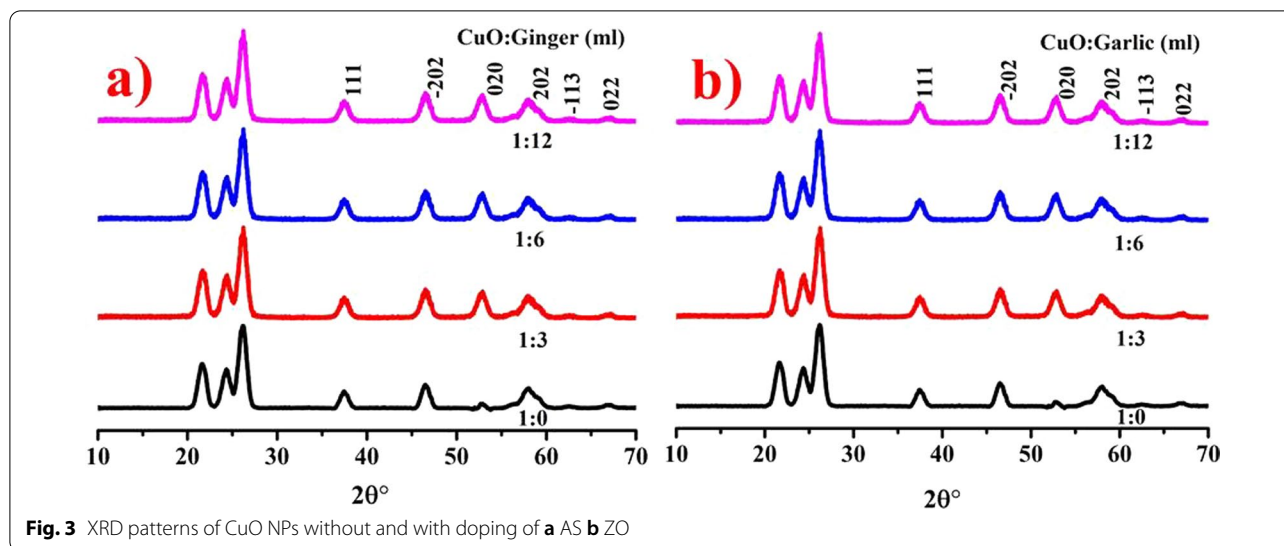


**Fig. 3** XRD patterns of CuO NPs without and with doping of **a** AS **b** ZO

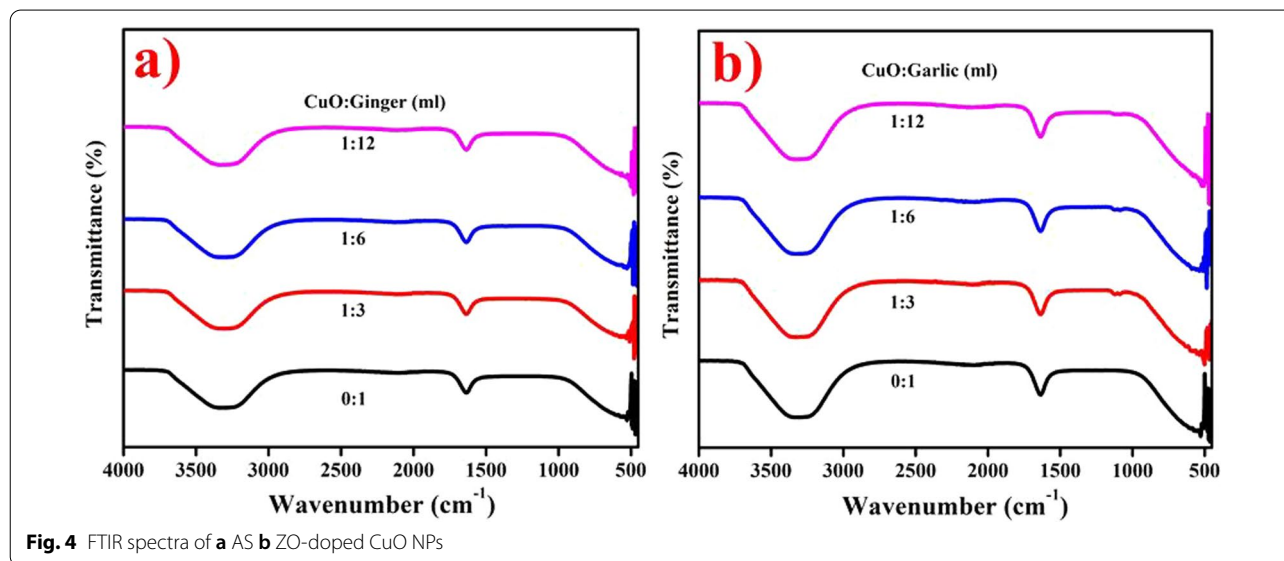


**Fig. 4** FTIR spectra of **a** AS **b** ZO-doped CuO NPs

Functional groups of AS and ZO extract doped CuO NPs were examined with FTIR as illustrated in Fig. 4a, b, correspondingly. The broad peak at  $3314\text{ cm}^{-1}$  endorsed the presence of hydroxyl group and peak wideness represents direct C=O with (N–H) amines [45]. The intense peak at  $1638\text{ cm}^{-1}$  corresponded to  $\text{CH}_2\text{-OCH}_3$  group existing in 6-snogal and 6-gingerol of ZO as found substantial reduction of CuO. The typical single bonds of Cu–O seen at  $478.8\text{ cm}^{-1}$  in the twisting fashion were due to strong modes of vibration [46]. All peaks suggest that alcohol, amine and ketone groups resulted in chelation and capping of flavonoids, plant chemical substances and proteins [47].

FE-SEM was used to study surface characteristics and scale of CuO NPs doped with ZO and AS extract as shown in Fig. 5a–d'. The FE-SEM images show that the CuO NPs are extremely agglomerated in spherical morphology. Magnetic interference and the conformity of polymers between particles may show agglomeration between particles [48]. ZO and AS doping with CuO was evident by the images showing cluster formation and particle size seems  $< 1\text{ }\mu\text{m}$  as illustrated in Fig. 5b–d'.

Energy-dispersive X-ray spectroscopy (EDS) illustrated the chemical composition with elemental investigation of pristine sample and doped CuO NPs with ZO and AS root extracts by inveterate CuO phases as shown in

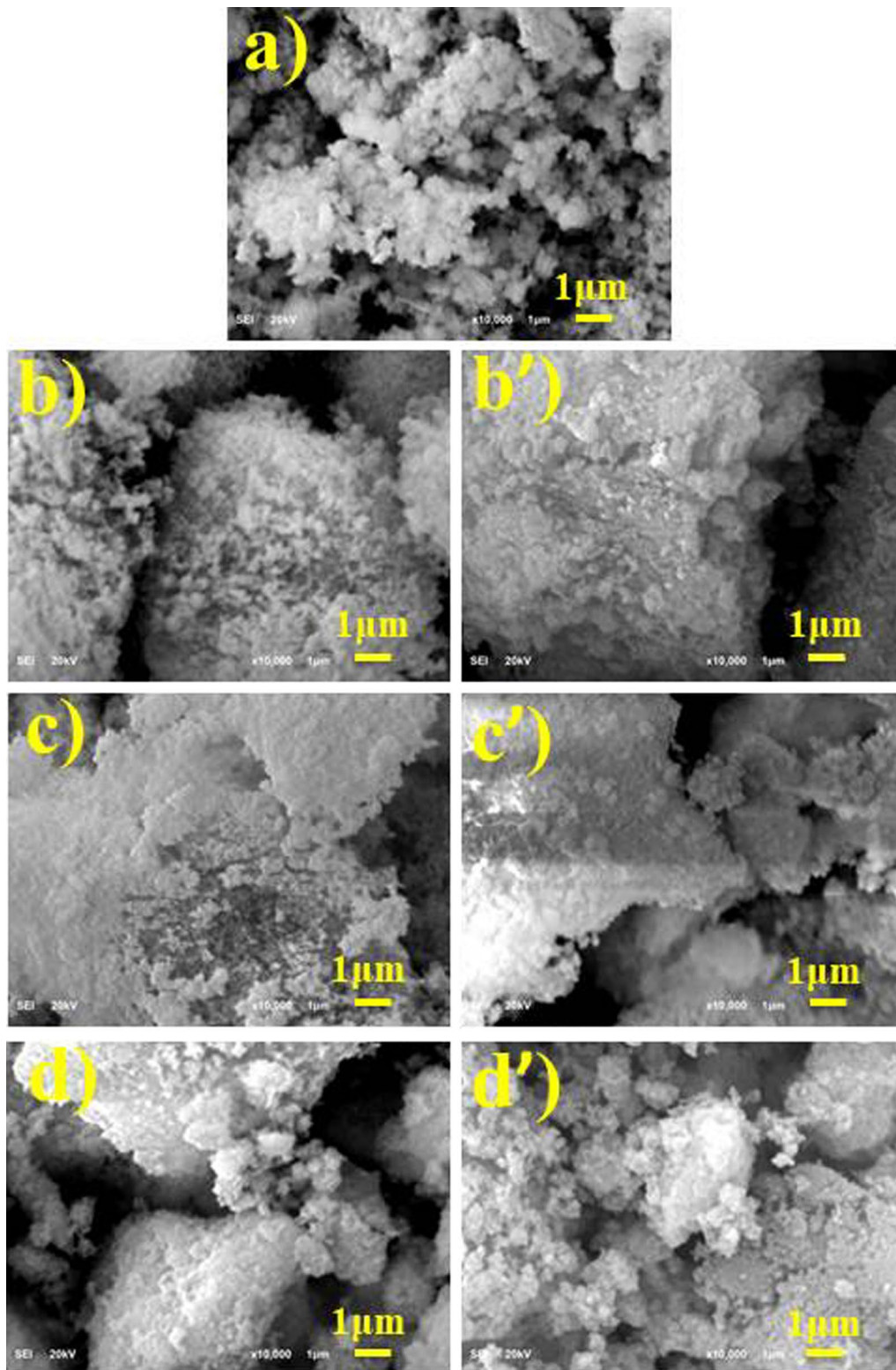


**Fig. 5** Images CuO NPs taken with FESEM **a** CuO, **b–d** ZO-doped CuO and **b'–d'** AS-doped CuO NPs, respectively



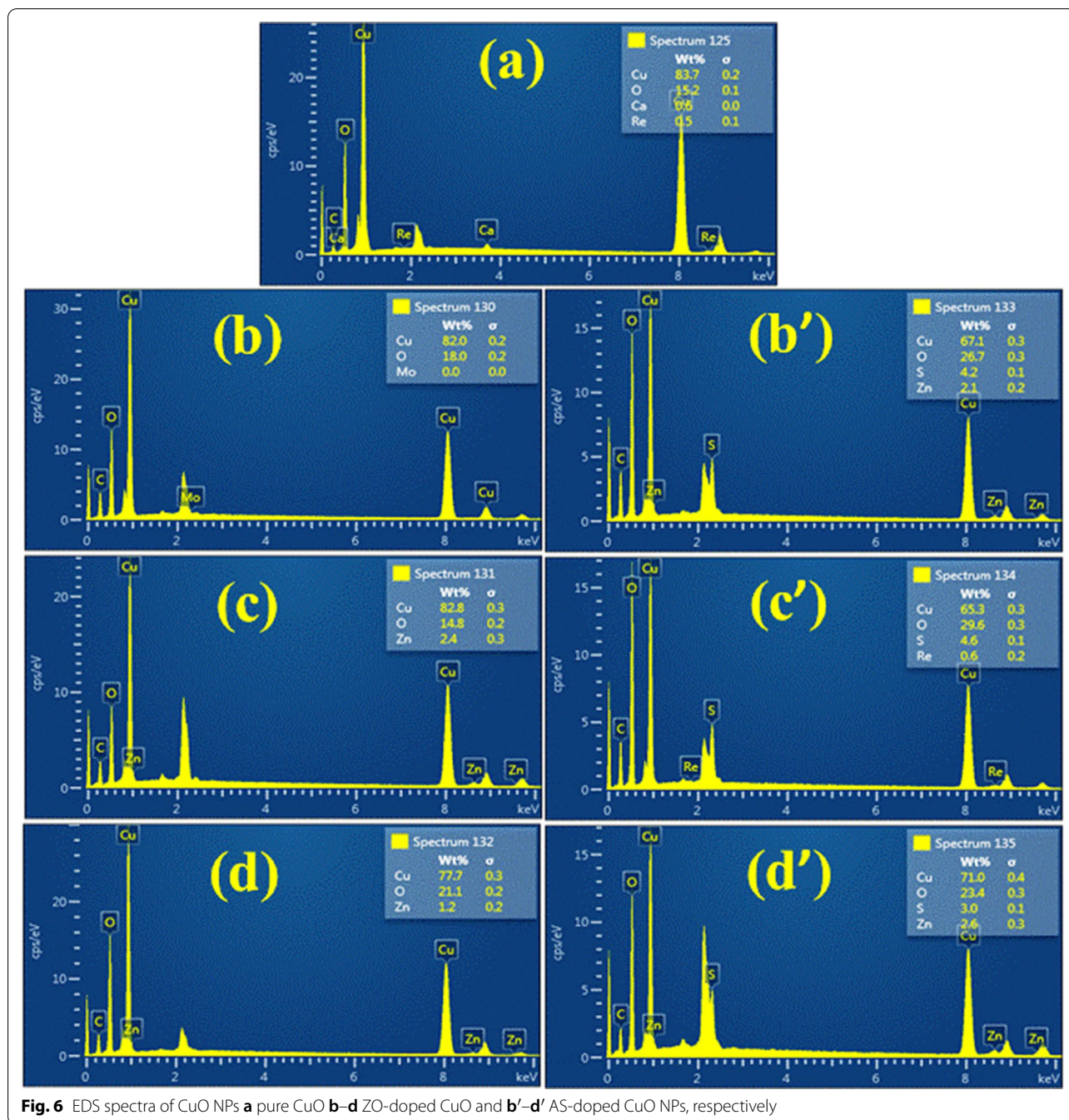
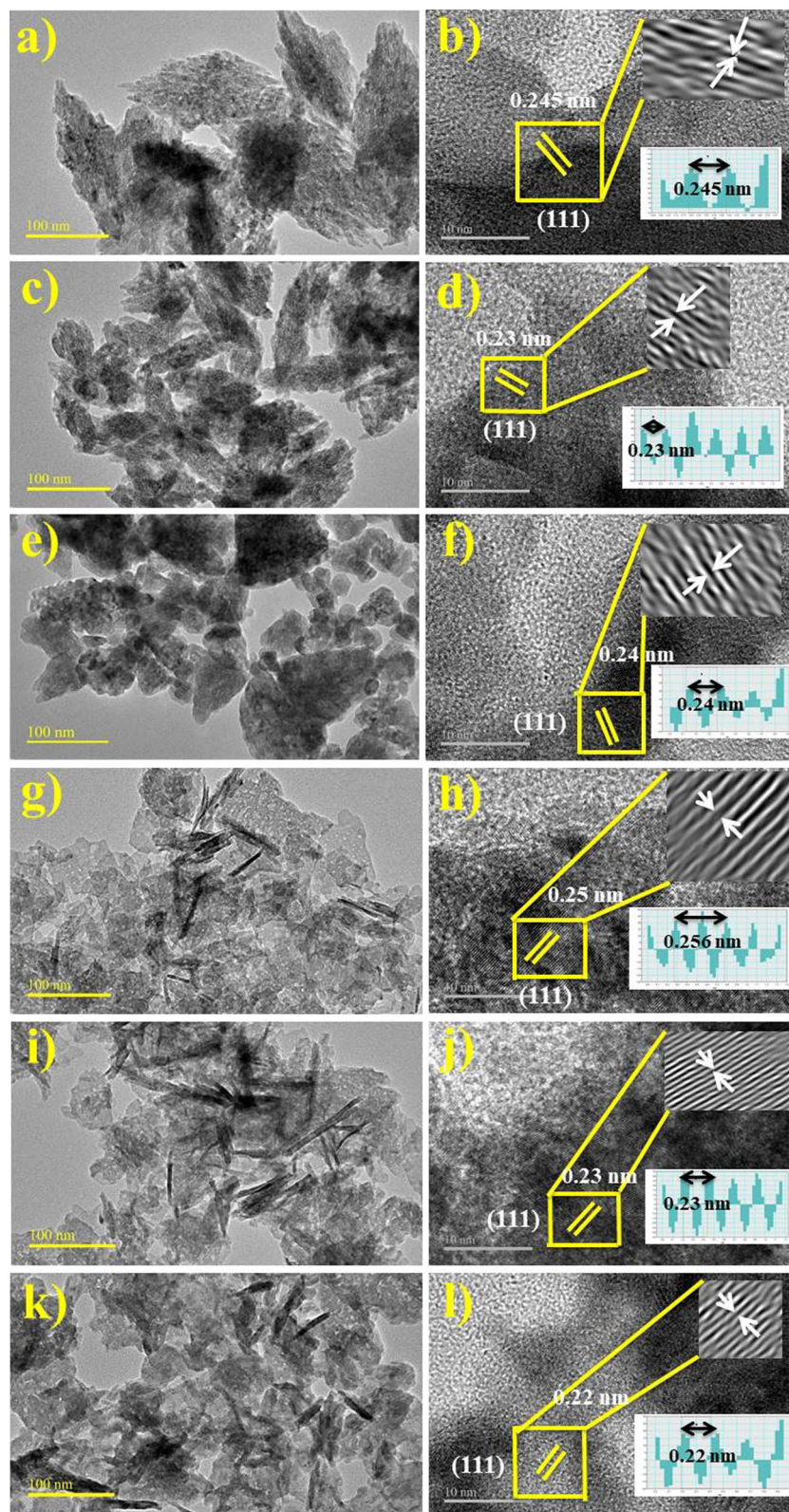


Fig. 6a–d'. Three peaks corresponding to the high purity of Cu confirmed by EDS of the samples tested in comparison with precursor oxygen between 1 and 10 keV. CuO NPs surface plasmon resonance (SPR) resulted in absorption peaks [49]. 83.7%, 15.2% and 0.6% were observed for atomic weight through spectra for Cu, O and Ca, respectively, for control sample whereas 82.8%, 14.8% and 2.4% for the ZO-doped and optimized sample (6 mL:1) observed through spectra for Cu, O and Zn, respectively.

Similarly, 65.3, 29.6 and 4.6 for Cu, O and S with AS doping were found, respectively. The supplementary atomic compounds appearing in EDS responded to SEM sample holder used during analysis [50].

The exclusive and characteristic structure of CuO NPs was further assessed using HR-TEM at 50 nm as displayed in Fig. 7a–l. HR-TEM pictures revealed adorned nanoparticles similar to FE-SEM images, along with higher agglomeration while size measuring less than





**Fig. 7** a, b HR-TEM, a–f lattice fringes of 3 mL, 6 mL and 12 mL ZO-doped CuO g–l lattice fringes of 3 mL, 6 mL and 12 mL AS-doped CuO NPs, respectively



50 nm. The presence of phytochemicals in ZO- and AS-doped CuO NPs were also confirmed with HR-TEM images [51]. Neither any imperfection nor any deformity was observed in the integral lattice structure of ZO- and AS-doped CuO NPs [52]. Filtered micrographs were presented by HR-TEM results along with fast Fourier transform [FFT] of specified area depicted by yellow square in Fig. 7b, d, f, h, j, l presenting high resolution structural and atomic characteristics. The HR-TEM mean particulate dimensions are precisely matched to the crystallite sizes observed during XRD and SEM analysis [53].

The XPS analysis of doped CuO with Gi and Ga CAE depicting C 1s and Cu 2p spectrum is shown in Fig. 8a, b. The C1s range indicated presence of four distinct peaks Fig. 8a with distinctive functional groups as C(H,C) (284.39 eV), C(N) (285.6 eV), C(O,=N) (287.0 eV) and C–O–C (288.75 eV) [54–56]. Mainly, Fig. 8b depicted Cu 2p pattern of doped CuO with peaks at 933.3 and 953.3 eV binding energies corresponding to Cu 2p<sub>3/2</sub> and Cu 2p<sub>1/2</sub> spin orbit indicates divalent oxidation state of prepared sample. The relevant peaks at 942.2 and 962 eV relate to satellite peaks of Cu 2p<sub>3/2</sub> and Cu 2p<sub>1/2</sub> which seemed mainly due to partially filled 3d<sup>9</sup> orbital in divalent oxidation state [57].

Well diffusion method was applied for the evaluation of bactericidal potential of ZO and AS aqueous extracts and synthesized CuO NPs by measuring inhibition areas after incubating the petri plates for 24 h as shown in Fig. 9a–d, Additional file 1: Fig. S1 and tabulated in Table 1. The findings revealed that the NPs concentration and inhibiting zones responded synergistically. Significant inhibition zones found for sample 1 (3 mL:1), sample 2 (6 mL:1) and sample 3 (12 mL:1) were (1.05–1.85 mm) and (1.85–2.30 mm) using decreased (↓) and increased (↑) concentrations, respectively, for ZO-doped CuO

nanoparticles ( $p < 0.05$ ), Fig. 9a. Similarly, AS-doped NPs exhibited (0.65–1.00 mm) inhibition zones at maximum concentration only, Fig. 9b. AS-doped NPs demonstrated zero efficacy against pathogenic *E. coli* at minimum concentrations. ZO extract depicted effect at decreased (↓) concentration in comparison to increased (↑) concentration showing 1.55 mm zone, similarly, no antibacterial effect of AS extracts was found at both decreased (↓) and increased (↑) concentrations. The control positive treated with ciprofloxacin showed 4.25 mm zone while control negative treated with DIW exhibited 0 mm. The bactericidal efficacy %age was raised from 24.7 to 43.5% and 43.5–54.1% for ZO-doped NPs at minimum and maximum concentrations, respectively (Fig. 9c). Similarly, 15.3–23.5% efficacy resulted at maximum concentration only for AS-doped NPs (Fig. 9d). In summary, CuO doped with ZO extract and optimized at 6 mL:1 manifested higher bactericidal potential against pathogenic *E. coli* of bovine mastitis origin ( $p < 0.05$ ) as shown in Fig. 9a, b.

Bactericidal potential of nanoparticles is dependent on the size of NPs, morphological structure and surface-to-mass ratio. Reactive oxygen species (ROS) are thought to be responsible for the formation of zones of inhibition by CuO nanoparticles [58, 59]. Denaturation of cell protein resulted through generation of detrimental reactive oxygen species (ROS) [60]. Some reactive species exhibited momentous roles in the photocatalysis such as hydroxyl and superoxide radicals and holes [61]. Synthesis of reactive oxygen species (ROS) and release of metal ions are the major features manifesting the structural changes of enzymes and proteins consequently resulting in irreparable damage to DNA and subsequent bacterial death [62]. Similarly, oxidative stress produced by reactive oxygen species (ROS)

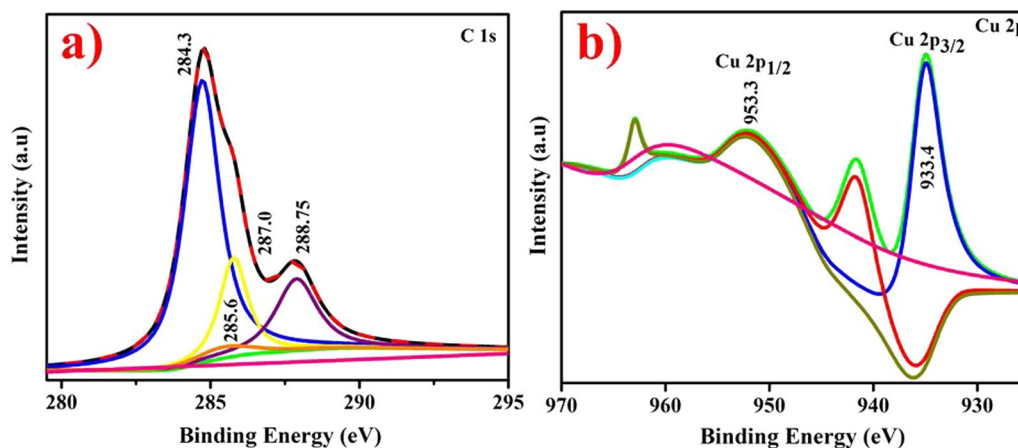


**Fig. 8** a, b XPS analysis of doped CuO NPs a C1s b Cu 2p

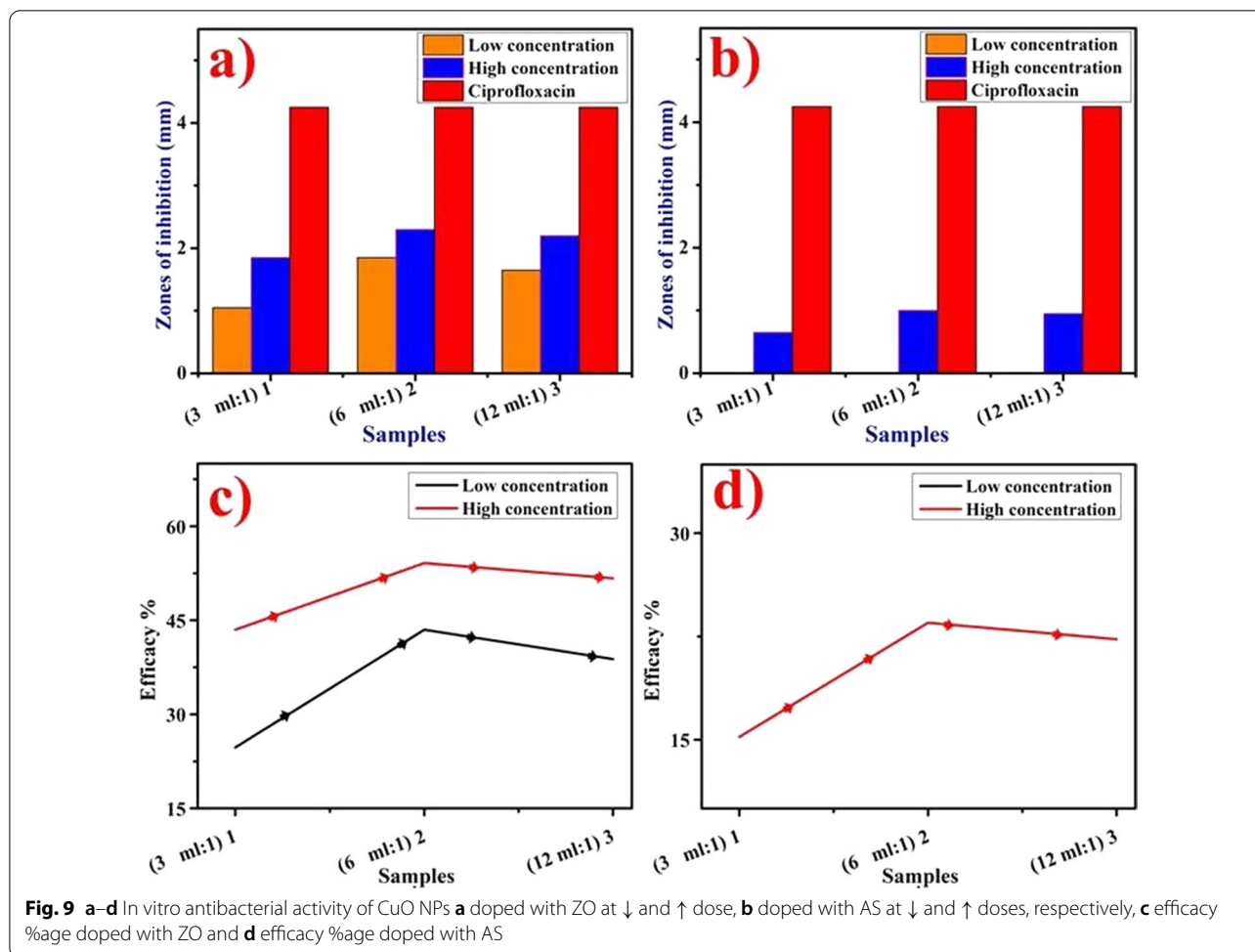


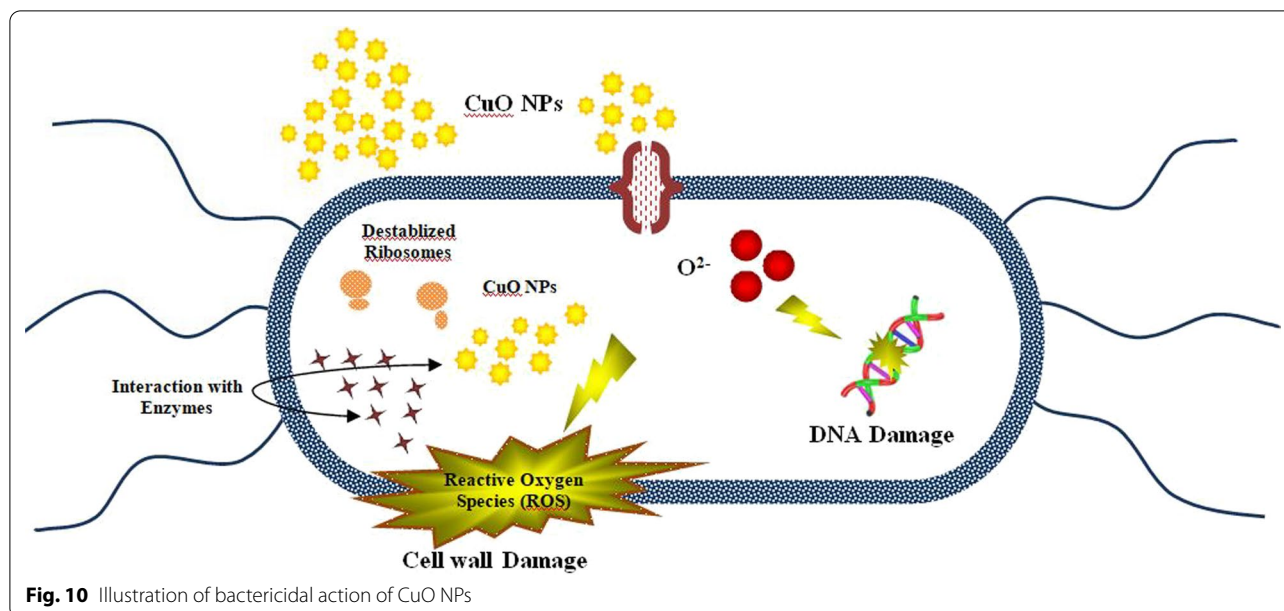
**Table 1** Bactericidal activity

Etiology	Material	500 µg/50 µl					1000 µg/50 µl				
		1	2	3	4	5	1	2	3	4	5
Pathogenic <i>E. coli</i>	ZO:CuO	1.05	1.85	1.65	4.25	0	1.85	2.3	2.2	4.25	0
	AS:CuO	0	0	0	4.25	0	0.65	1	0.95	4.25	0

<sup>1</sup> (3 mL:1), <sup>2</sup>(6 mL:1), <sup>3</sup>(12 mL:1), <sup>4</sup>Ciprofloxacin, <sup>5</sup>DIW

is considered to be the major contributor to photocatalysis [63]. ROS production is inversely proportional to the size of nanoparticles, i.e., smaller the size of NPs, higher is the ROS production which consequently damages the bacterial membrane resulting in extrusion of cytoplasmic contents and DNA degradation leading to bacterial burst as portrayed in Fig. 10. At the same time, positively charged Cu interacts electrostatically with negatively charged bacterial membrane resulting in cell disintegration and finally bacterial destruction [58, 64, 65]. Two responses have been proposed as

potential for the bactericidal mechanism of nanostructures. One involves better linkage between the cations  $\text{Cu}^{2+}$  and bacterial cells, leading to the formation of negativized sections and eventual collapse. The other involves electronic excitation of the CuO valance band surface via excitation. Furthermore, the electrical  $\text{O}_2$  reaction produces  $\text{O}^{2-}$  radicals, leading to the formation of  $\text{H}_2\text{O}_2$ . The generated  $\text{O}^{2-}$  species are essential for the breakdown of lipid or protein molecules on the exterior cell membrane of bacteria [58, 66].



## Conclusions

Bactericidal potential of CuO NPs doped with *Zingiber officinale* and *Allium sativum* extracts against pathogenic *E. coli* was evaluated in this study, produced with the aim of alternate, economical and effective antimicrobials. The significant role of phytochemical ingredients of ZO and AS extracts was revealed in the biogenic synthesis of CuO NPs while synergistic effects of flavonoids with CuO were found to be concentration-dependent exploiting the bactericidal potential against pathogenic *E. coli*. FTIR was performed for confirmation of ZO and AS extracts doping and XRD peaks confirmed the monoclinic phase and spherical structure with mean sizes 24.7 nm (ZO-doped) and 47.6 nm (AS-doped). Spherical morphology was confirmed with FESEM images along with an exorbitant conglomeration of CuO NPs. Embellished nanoparticles revealed higher agglomeration in TEM images with size of less than 50 nm. For doped samples with root extracts, interlayer spacing of CuO nanoparticles measured as 0.23 nm was found compatible with XRD patterns. The results of this study suggest that antibacterial potential of green synthesized CuO NPs may be anticipated as alternate bactericidal agents to redress the concerns related to antibiotics resistance and residues. It may be concluded that CuO NPs doped with indigenous herbs are economical, effective and nature-friendly antibacterial agents.

## Abbreviations

EDS: Energy-dispersive X-ray spectroscopy; fcc: Face-centered cubic; FTIR: Fourier transform infrared spectroscopy; G + ve: Gram positive; G -ve: Gram negative; JCPDS: Joint committee on powder diffraction standards; CuO: Copper oxide; nm: Nanometer.

## Supplementary Information

The online version contains supplementary material available at <https://doi.org/10.1186/s11671-021-03605-z>.

**Additional file 1: Fig. S1.** (a–d) In-vitro antibacterial activity of doped CuO NPs (a, b) Gi doped CuO at ↓ and ↑ dose, (c, d) Ga doped CuO at ↓ and ↑ doses, respectively

## Acknowledgements

Support provided by the Core Research Facilities at King Fahd University of Petroleum and Minerals, Dhahran, Saudi Arabia, is highly appreciated.

## Authors' contributions

MA performed the whole experiments and wrote the manuscript. MI provided the novel idea to carry out the experiment. MI, MA and AAA participated in the data analysis of the results and discussion portion. AUH reviewed the manuscript, corrected the English and carried out the FESEM and HRTEM analysis. All authors read and approved the final manuscript.

## Funding

The authors are thankful to HEC, Pakistan, through Project 21-1669/SRGP/R&D/HEC/2017.

## Availability of data and materials

All data are fully available without restriction.

## Declarations

### Competing interests

The authors declare that they have no competing interests.

### Author details

<sup>1</sup>Department of Veterinary Medicine, University of Veterinary and Animal Sciences, Lahore, Punjab 54000, Pakistan. <sup>2</sup>Solar Cell Applications Research Lab, Department of Physics, Government College University Lahore, Lahore, Punjab 54000, Pakistan. <sup>3</sup>Core Research Facilities, King Fahd University of Petroleum and Minerals, Dhahran 31261, Saudi Arabia.

Received: 29 April 2021 Accepted: 12 September 2021

Published online: 20 September 2021



## References

- Lopes TS, Fontoura PS, Oliveira A, Rizzo FA, Silveira S, Streck AF (2020) Use of plant extracts and essential oils in the control of bovine mastitis. *Res Vet Sci* 131:186–193
- Shin J, Prabhakaran VS, Kim KS (2018) The multi-faceted potential of plant-derived metabolites as antimicrobial agents against multidrug-resistant pathogens. *Microb Pathog* 116:209–214
- Mao QQ, Xu XY, Cao SY, Gan RY, Corke H, Li HB (2019) Bioactive compounds and bioactivities of ginger (*Zingiber officinale* Roscoe). *Foods* 8(6):185
- Amalraj A, Raj KJ, Haponiuk JT, Thomas S, Gopi S (2020) Preparation, characterization, and antimicrobial activity of chitosan/gum arabic/polyethylene glycol composite films incorporated with black pepper essential oil and ginger essential oil as potential packaging and wound dressing materials. *Adv Compos Hybrid Mater* 3(4):485–497
- Magryś A, Olender A, Tchórzewska D (2021) Antibacterial properties of *Allium sativum* L. against the most emerging multidrug-resistant bacteria and its synergy with antibiotics. *Arch Microbiol* 203:227–2268
- Agi VN, Azike CA (2019) Antifungal action of garlic (*Allium sativum*) and Ginger (*Zingiber officinale*) on some pathogenic fungi. *Asian J Res Biochem*. <https://doi.org/10.9734/ajrb/2019/v4i430075>
- Chenthamara D, Subramaniam S, Ramakrishnan SG, Krishnaswamy S, Essa MM, Lin FH, Qoronfleh MW (2019) Therapeutic efficacy of nanoparticles and routes of administration. *Biomater Res* 23(1):1–29
- Ameta SK, Rai AK, Hiran D, Ameta R, Ameta SC (2020) Use of nanomaterials in food science. In: Ghorbanpour M, Bhargava P, Varma A, Choudhary DK (eds) *Biogenic nano-particles and their use in agro-ecosystems*. Springer, Singapore, pp 447–488
- Alfei S, Marengo B, Zuccari G (2020) Nanotechnology application in food packaging: a plethora of opportunities versus pending risks assessment and public concerns. *Food Res Int* 137:109664
- Wang L, Hu C, Shao L (2017) The antimicrobial activity of nanoparticles: present situation and prospects for the future. *Int J Nanomed* 12:1227
- Zou X, Fan H, Tian Y, Yan S (2014) Synthesis of Cu<sub>2</sub>O/ZnO hetero-nanorod arrays with enhanced visible light-driven photocatalytic activity. *Cryst-EngComm* 16(6):1149–1156
- Zou X, Fan H, Tian Y, Zhang M, Yan X (2015) Microwave-assisted hydrothermal synthesis of Cu/Cu<sub>2</sub>O hollow spheres with enhanced photocatalytic and gas sensing activities at room temperature. *Dalton Trans* 44(17):7811–7821
- Zou X, Fan H, Tian Y, Zhang M, Yan X (2015) Chemical bath deposition of Cu<sub>2</sub>O quantum dots onto ZnO nanorod arrays for application in photovoltaic devices. *RSC Adv* 5(30):23401–23409
- Zhai Y, Fan H, Li Q, Yan W (2012) Morphology evolutions and optical properties of Cu<sub>2</sub>O films by an electrochemical deposition on flexible substrate. *Appl Surf Sci* 258(7):3232–3236
- Singh R, Cheng S, Singh S (2020) Oxidative stress-mediated genotoxic effect of zinc oxide nanoparticles on *Deinococcus radiodurans*. *3 Biotech* 10(2):1–13
- Gamboa SM, Rojas ER, Martínez VV, Vega-Baudrit J (2019) Synthesis and characterization of silver nanoparticles and their application as an antibacterial agent. *Int J Biosens Bioelectron* 5:166–173
- Zhang D, Ma XL, Gu Y, Huang H, Zhang GW (2020) Green synthesis of metallic nanoparticles and their potential applications to treat cancer. *Front Chem*. <https://doi.org/10.3389/fchem.2020.00799>
- LeStrange K, Markland SM, Hoover DG, Sharma M, Kniel KE (2017) An evaluation of the virulence and adherence properties of avian pathogenic *Escherichia coli*. *One Health* 4:22–26
- Khan SA, Imtiaz MA, Sayeed MA, Shaikat AH, Hassan MM (2020) Antimicrobial resistance pattern in domestic animal-wildlife-environmental niche via the food chain to humans with a Bangladesh perspective; a systematic review. *BMC Vet Res* 16(1):1–13
- Zhang Y, Gu AZ, Cen T, Li X, He M, Li D, Chen J (2018) Sub-inhibitory concentrations of heavy metals facilitate the horizontal transfer of plasmid-mediated antibiotic resistance genes in water environment. *Environ Pollut* 237:74–82
- Sodagari HR, Wang P, Robertson I, Abraham S, Sahibzada S, Habib I (2021) Antimicrobial resistance and genomic characterisation of *Escherichia coli* isolated from caged and non-caged retail table eggs in Western Australia. *Int J Food Microbiol* 340:109054
- Goswami C, Fox S, Holden MT, Connor M, Leanord A, Evans TJ (2020) Origin, maintenance and spread of antibiotic resistance genes within plasmids and chromosomes of bloodstream isolates of *Escherichia coli*. *Microb Genomics*. <https://doi.org/10.1099/mgen.0.000353>
- Ali M, Ikram M, Ijaz M, Ul-Hamid A, Avais M, Anjum AA (2020) Green synthesis and evaluation of n-type ZnO nanoparticles doped with plant extract for use as alternative antibacterials. *Appl Nanosci* 10:3787–3803
- Roussel P, Porcherie A, Répérant-Ferret M, Cunha P, Gittton C, Rainard P, Germon P (2017) *Escherichia coli* mastitis strains: in vitro phenotypes and severity of infection in vivo. *PLoS ONE* 12(7):e0178285
- Ali T, Ur Rahman S, Zhang L, Shahid M, Han D, Gao J, Zhang S, Ruegg PL, Saddique U, Han B (2017) Characteristics and genetic diversity of multidrug resistant extended-spectrum beta-lactamase (ESBL)-producing *Escherichia coli* isolated from bovine mastitis. *Oncotarget* 8(52):90144
- Kose A, Colak C (2021) Knowledge levels and awareness about rational antibiotic use and antimicrobial resistance before and after graduation: a cross-sectional study conducted in Malatya province, Turkey. <https://doi.org/10.21203/rs.3.rs-365360/v1>
- Kumar AS, Madhu G, John E, Kuttinarayanan SV, Nair SK (2020) Optical and antimicrobial properties of silver nanoparticles synthesized via green route using honey. *Green Process Synth* 9(1):268–274
- Salam HA, Sivaraj R, Venkatesh R (2014) Green synthesis and characterization of zinc oxide nanoparticles from *Ocimum basilicum* L. var. *purpurascens* Benth.-Lamiaceae leaf extract. *Mater Lett* 131:16–18
- Fakhari S, Jamzad M, Kabiri Fard H (2019) Green synthesis of zinc oxide nanoparticles: a comparison. *Green Chem Lett Rev* 12(1):19–24
- Kumar B, Smita K, Cumbal L, Debut A, Angulo Y (2017) Biofabrication of copper oxide nanoparticles using Andean blackberry (*Rubus glaucus* Benth.) fruit and leaf. *J Saudi Chem Soc* 21:S475–S480
- Baqer AA, Matori KA, Al-Hada NM, Kamari HM, Shaari AH, Saion E, Chyi JLY (2018) Copper oxide nanoparticles synthesized by a heat treatment approach with structural, morphological and optical characteristics. *J Mater Sci: Mater Electron* 29(2):1025–1033
- Rabiee N, Bagherzadeh M, Kiani M, Ghadiri AM, Etesamiyar F, Jaberizadeh AH, Shakeri A (2020) Biosynthesis of copper oxide nanoparticles with potential biomedical applications. *Int J Nanomed* 15:3983
- Baban ST (2019) Prevalence and antimicrobial susceptibility pattern of extended spectrum beta-lactamase-producing *Escherichia coli* isolated from urinary tract infection among infants and young children in Erbil City. *J Med Sci* 23(3):3251–3258
- Sharma R, Lambu MR, Jamwal U, Rani C, Chib R, Wazir P, Mukherjee D, Chaubey A, Khan IA (2016) *Escherichia coli* N-acetylglucosamine-1-phosphate-uridylyltransferase/glucosamine-1-phosphate-acetyltransferase (GlmU) inhibitory activity of terreic acid isolated from *Aspergillus terreus*. *J Biomol Screen* 21(4):342–353
- Nasrollahzadeh M, Sajadi SM, Rostami-Vartooni A, Hussin SM (2016) Green synthesis of CuO nanoparticles using aqueous extract of *Thymus vulgaris* L. leaves and their catalytic performance for N-arylation of indoles and amines. *J Colloid Interface Sci* 466:113–119
- Endres J, Egger DA, Kulbak M, Kerner RA, Zhao L, Silver SH, Hodes G, Rand BP, Cahen D, Kronik L, Kahn A (2016) Valence and conduction band densities of states of metal halide perovskites: a combined experimental–theoretical study. *J Phys Chem Lett* 7(14):2722–2729
- Sone BT, Diallo A, Fuku XG, Gurib-Fakim A, Maaza M (2020) Biosynthesized CuO nano-platelets: physical properties & enhanced thermal conductivity nanofluidics. *Arab J Chem* 13(1):160–170
- Chang SS, Lee HJ, Park HJ (2005) Photoluminescence properties of spark-processed CuO. *Ceram Int* 31(3):411–415
- Mukherjee N, Show B, Maji SK, Madhu U, Bhar SK, Mitra BC, Khan GG, Mondal A (2011) CuO nano-whiskers: electrodeposition, Raman analysis, photoluminescence study and photocatalytic activity. *Mater Lett* 65(21–22):3248–3250
- Mohamed RM, Harraz FA, Shawky A (2014) CuO nanobelts synthesized by a template-free hydrothermal approach with optical and magnetic characteristics. *Ceram Int* 40(1):2127–2133
- Sathyamoorthy R, Mageshwari K (2013) Synthesis of hierarchical CuO microspheres: photocatalytic and antibacterial activities. *Physica E* 47:157–161
- Huang CY, Chatterjee A, Liu SB, Wu SY, Cheng CL (2010) Photoluminescence properties of a single tapered CuO nanowire. *Appl Surf Sci* 256(11):3688–3692

43. Ahmed S, Mansoor MA, Mazhar M, Söhnel T, Khaledi H, Basirun WJ, Arifin Z, Abubakar S, Muhammad B (2014) Semiconducting composite oxide  $Y_2CuO_4$ -5CuO thin films for investigation of photoelectrochemical properties. *Dalton Trans* 43(22):8523–8529
44. Bhandari PR (2012) Garlic (*Allium sativum* L.): a review of potential therapeutic applications. *Int J Green Pharm (IJGP)* 6(2):118
45. Ahmed B, Hashmi A, Khan MS, Musarrat J (2018) ROS mediated destruction of cell membrane, growth and biofilms of human bacterial pathogens by stable metallic AgNPs functionalized from bell pepper extract and quercetin. *Adv Powder Technol* 29(7):1601–1616
46. Xu Y, Wang C, Chen D, Jiao X (2010) Fabrication and characterization of novel nanostructured copper oxide films via a facile solution route. *Mater Lett* 64(3):249–251
47. Shankar SS, Rai A, Ahmad A, Sastry M (2004) Rapid synthesis of Au, Ag, and bimetallic Au core–Ag shell nanoparticles using Neem (*Azadirachta indica*) leaf broth. *J Colloid Interface Sci* 275(2):496–502
48. Wang XS, Liu X, Wen L, Zhou Y, Jiang Y, Li Z (2008) Comparison of basic dye crystal violet removal from aqueous solution by low-cost biosorbents. *Sep Sci Technol* 43(14):3712–3731
49. Ramesh M, Anbuvarannan M, Viruthagiri GJSAPAM (2015) Green synthesis of ZnO nanoparticles using *Solanum nigrum* leaf extract and their antibacterial activity. *Spectrochim Acta A Mol Biomol Spectrosc* 136:864–870
50. Wang C, Kim YJ, Singh P, Mathiyalagan R, Jin Y, Yang DC (2016) Green synthesis of silver nanoparticles by *Bacillus methylotrophicus*, and their antimicrobial activity. *Artif Cells Nanomed Biotechnol* 44(4):1127–1132
51. Rajakumar G, Thiruvengadam M, Mydhili G, Gomathi T, Chung IM (2018) Green approach for synthesis of zinc oxide nanoparticles from *Andrographis paniculata* leaf extract and evaluation of their antioxidant, anti-diabetic, and anti-inflammatory activities. *Bioprocess Biosyst Eng* 41(1):21–30
52. Qi Y, Wang N, Xu Q, Li H, Zhou P, Lu X, Zhao G (2015) A green route to fabricate  $MoS_2$  nanosheets in water–ethanol– $CO_2$ . *Chem Commun* 51:6726–6729
53. Jadhav MS, Kulkarni S, Raikar P, Barretto DA, Vootla SK, Raikar US (2018) Green biosynthesis of CuO & Ag–CuO nanoparticles from *Malus domestica* leaf extract and evaluation of antibacterial, antioxidant and DNA cleavage activities. *New J Chem* 42(1):204–213
54. Hamza MF, Wei Y, Mira HI, Adel AH, Guibal E (2019) Synthesis and adsorption characteristics of grafted hydrazinyl amine magnetite–chitosan for Ni(II) and Pb(II) recovery. *Chem Eng J* 362:310–324
55. Jurado-López B, Vieira RS, Rabelo RB, Beppu MM, Casado J, Rodríguez-Castellón E (2017) Formation of complexes between functionalized chitosan membranes and copper: a study by angle resolved XPS. *Mater Chem Phys* 185:152–161
56. Ortega-Liebana MC, Chung NX, Limpens R, Gomez L, Hueso JL, Santamaria J, Gregorkiewicz T (2017) Uniform luminescent carbon nanodots prepared by rapid pyrolysis of organic precursors confined within nanoporous templating structures. *Carbon* 117:437–446
57. Poulston S, Parlett PM, Stone P, Bowker M (1996) Surface oxidation and reduction of CuO and Cu<sub>2</sub>O studied using XPS and XAES. *Surf Interface Anal* 24(12):811–820
58. Haider A, Ijaz M, Ali S, Haider J, Imran M, Majeed H, Shahzadi I, Ali MM, Khan JA, Ikram M (2020) Green synthesized phytochemically (*Zingiber officinale* and *Allium sativum*) reduced nickel oxide nanoparticles confirmed bactericidal and catalytic potential. *Nanoscale Res Lett* 15(1):1–11
59. Ikram M, Abbasi S, Haider A, Naz S, Ul-Hamid A, Imran M, Haider J, Ghaffar A (2020) Bimetallic Ag/Cu incorporated into chemically exfoliated  $MoS_2$  nanosheets to enhance its antibacterial potential: in silico molecular docking studies. *Nanotechnology* 31(27):275704
60. Zhang X, He X, Kang Z, Cui M, Yang DP, Luque R (2019) Waste eggshell-derived dual-functional CuO/ZnO/eggshell nanocomposites:(Photo) catalytic reduction and bacterial inactivation. *ACS Sustain Chem Eng* 7(18):15762–15771
61. Zhang X, Zhou J, Yang DP, Chen S, Huang J, Li Z (2019) Cu<sub>2</sub>-xS loaded diatom nanocomposites as novel photocatalysts for efficient photocatalytic degradation of organic pollutants. *Catal Today* 335:228–235
62. He X, Yang DP, Zhang X, Liu M, Kang Z, Lin C, Jia N, Luque R (2019) Waste eggshell membrane-templated CuO–ZnO nanocomposites with enhanced adsorption, catalysis and antibacterial properties for water purification. *Chem Eng J* 369:621–633
63. Zhang X, Huang J, Kang Z, Yang DP, Luque R (2020) Eggshell-templated synthesis of PbS/CaCO<sub>3</sub> nanocomposites for CO<sub>2</sub>—mediated efficient degradation of tetracycline under solar light irradiation. *Mol Catal* 484:110786–110791
64. Rashid M, Ikram M, Haider A, Naz S, Haider J, Ul-Hamid A, Shahzadi A, Aqeel M (2020) Photocatalytic, dye degradation, and bactericidal behavior of Cu-doped ZnO nanorods and their molecular docking analysis. *Dalton Trans* 49(24):8314–8330
65. Ikram M, Umar E, Raza A, Haider A, Naz S, Ul-Hamid A, Haider J, Shahzadi I, Hassan J, Ali S (2020) Dye degradation performance, bactericidal behavior and molecular docking analysis of Cu-doped TiO<sub>2</sub> nanoparticles. *RSC Adv* 10(41):24215–24233
66. Rajan PI, Vijaya JJ, Jesudoss SK, Kaviyarasu K, Kennedy LJ, Jothiramingam R, Al-Lohedan HA, Vaali-Mohammed MA (2017) Green-fuel-mediated synthesis of self-assembled NiO nano-sticks for dual applications—photocatalytic activity on Rose Bengal dye and antimicrobial action on bacterial strains. *Mater Res Express* 4(8):085030

## Publisher's Note

Springer Nature remains neutral with regard to jurisdictional claims in published maps and institutional affiliations.

Submit your manuscript to a SpringerOpen® journal and benefit from:

- Convenient online submission
- Rigorous peer review
- Open access: articles freely available online
- High visibility within the field
- Retaining the copyright to your article

Submit your next manuscript at ► [springeropen.com](https://www.springeropen.com)